The Cryosphere, 16, 4537–4552, 2022
https://doi.org/10.5194/tc-16-4537-2022
© Author(s) 2022. This work is distributed under
the Creative Commons Attribution 4.0 License.

The Cryosphere
Open Access

Subglacial hydrology modulates basal sliding response of the Antarctic ice sheet to climate forcing

Elise Kazmierczak[1], **Sainan Sun**[1,2], **Violaine Coulon**[1], **and Frank Pattyn**[1]

[1]Laboratoire de Glaciologie, Université libre de Bruxelles (ULB), Brussels, Belgium
[2]Department of Geography and Environmental Sciences, Northumbria University, Newcastle upon Tyne, UK

Correspondence: Elise Kazmierczak (elise.kazmierczak@ulb.be)

Received: 2 March 2022 – Discussion started: 29 March 2022
Revised: 12 August 2022 – Accepted: 19 September 2022 – Published: 27 October 2022

Abstract. Major uncertainties in the response of ice sheets to environmental forcing are due to subglacial processes. These processes pertain to the type of sliding or friction law as well as the spatial and temporal evolution of the effective pressure at the base of ice sheets. We evaluate the classic Weertman–Budd sliding law for different power exponents (viscous to near plastic) and for different representations of effective pressure at the base of the ice sheet, commonly used for hard and soft beds. The sensitivity of the above slip laws is evaluated for the Antarctic ice sheet in two types of experiments: (i) the ABUMIP experiments in which ice shelves are instantaneously removed, leading to rapid grounding-line retreat and ice sheet collapse, and (ii) the ISMIP6 experiments with realistic ocean and atmosphere forcings for different Representative Concentration Pathway (RCP) scenarios. Results confirm earlier work that the power in the sliding law is the most determining factor in the sensitivity of the ice sheet to climatic forcing, where a higher power in the sliding law leads to increased mass loss for a given forcing. Here we show that spatial and temporal changes in water pressure or water flux at the base modulate basal sliding for a given power, especially for high-end scenarios, such as ABUMIP. In particular, subglacial models depending on subglacial water pressure decrease effective pressure significantly near the grounding line, leading to an increased sensitivity to climatic forcing for a given power in the sliding law. This dependency is, however, less clear under realistic forcing scenarios (ISMIP6).

1 Introduction

The Antarctic ice sheet (AIS) is the biggest freshwater store on Earth (Fretwell et al., 2013; Rignot et al., 2019) and has been losing mass at an accelerating pace due to an increased ice discharge from the West Antarctic ice sheet (WAIS; Rignot et al., 2019; Shepherd et al., 2019). Future mass loss of the ice sheet represents the largest source of uncertainty with respect to future sea level rise (Kopp et al., 2014, 2017; Frederikse et al., 2020). Major uncertainties pertain to the interaction of the Antarctic ice sheet with the ocean (Alley et al., 2015; Scambos et al., 2017; de Boer et al., 2017; Asay-Davis et al., 2017), but this interaction is modulated by internal ice sheet dynamics that govern the rate and magnitude of ice sheet mass change in response to changes at the marine boundary. Internal ice sheet dynamics are dominated by the basal conditions of the ice sheet and more precisely the amount and type of basal sliding that takes place (Pattyn, 1996; Ritz et al., 2015; Pattyn, 2017; Bulthuis et al., 2019; Joughin et al., 2019; Sun et al., 2020). Especially, the contrast between viscous (linear) and plastic (Coulomb) sliding laws makes the latter far more responsive to changes at the marine boundary. In addition to the sliding type, physical basal conditions, such as basal temperature, bed properties (hard or soft), subglacial water flow and drainage, or till properties and mechanics, add to the sensitivity of the ice sheet to climatic forcing (Clarke, 2005; Cuffey and Paterson, 2010). While the presence of subglacial water leads to lubrication between the ice and the bed, high subglacial water pressure is implicated in persistent and episodic fast ice flow processes (Bindschadler, 1983; Tulaczyk et al., 2000). However, few have attempted to establish physical laws coupling

subglacial hydrology and basal sliding on a large scale, such as ice sheets (Flowers, 2015).

Nevertheless, our understanding of subglacial processes has greatly improved, both from a theoretical viewpoint (Schoof et al., 2012; Hewitt et al., 2012) and through the development of high-resolution subglacial hydrological models (Flowers and Clarke, 2002a; Hewitt, 2011; Werder et al., 2013; Fleurian et al., 2014; Hoffman and Price, 2014; Bueler and van Pelt, 2015; Brinkerhoff et al., 2016; Beyer et al., 2018; Gagliardini and Werder, 2018; Sommers et al., 2018), eventually leading to the first subglacial model intercomparison SHMIP (de Fleurian et al., 2018). Despite these efforts, applying subglacial models on the scale of ice sheets remains challenging due to the large computational demand and remains therefore mostly limited to individual basins on short timescales (Bougamont et al., 2014; Dow et al., 2016). In addition, the ability to resolve subglacial processes is often limited by the coarse spatial and temporal scales used in models; hence large-scale representations of such processes are usually implemented in continental-scale ice sheet models (Le Brocq et al., 2009; Flowers, 2015). Moreover, the lack of direct observations or precise measurements of the subglacial system makes their understanding particularly difficult. Many models deal with the hydrological system in an implicit way through data assimilation of observed satellite velocities to retrieve spatially varying basal friction coefficients. While this leads to improved initial conditions of the ice sheet, it does not allow for temporal changes in the hydrological system or the gauging of their effect on the sliding behaviour of the ice sheet.

Here, we consider four different ways, commonly found in the literature and generally used in large-scale ice sheet models, to link the hydrology to sliding at the base of ice sheets (Alley, 1989; Bueler and Brown, 2009; Winkelmann et al., 2011; Bueler and van Pelt, 2015; Goeller et al., 2013). They encompass the presence of a water film (Weertman, 1957; Le Brocq et al., 2009) across a rigid bed made of non-deforming rock (a "hard" bed) and the deformation of a saturated till layer (a "soft" bed) (Bueler and van Pelt, 2015; Muto et al., 2019). The effective pressure is then used as a state variable in the common Weertman–Budd (Weertman, 1957; Budd and Jenssen, 1987) sliding law for different exponents of the power law. Using the f.ETISh ice sheet model of intermediate complexity (Pattyn, 2017; Pelletier et al., 2022), centennial-scale simulations are performed for the ISMIP6 (Seroussi et al., 2020) and ABUMIP (Sun et al., 2020) setups. Results are subsequently analysed for the whole ice sheet as well as for separate drainage basins in view of their different characteristics (marine basins, hard/soft bed, land-based ice sheet, etc.).

2 Model description

We employed f.ETISh v.1.6 (Pattyn, 2017; Pelletier et al., 2022), which is a vertically integrated hybrid ice sheet–ice shelf model with full thermomechanical coupling. It combines the shallow-ice and shallow-shelf equations similarly to Winkelmann et al. (2011). Input data are the present-day ice sheet surface and bed geometry from BedMachine (Morlighem et al., 2020), surface mass balance and temperature from RACMO2 (Van Wessem et al., 2014), and a prescribed field for the geothermal heat flux (Shapiro and Ritzwoller, 2004). All datasets were resampled at a spatial resolution of 25 km.

The model uses a power law for basal sliding (Weertman, 1957; Budd et al., 1979; Budd and Jenssen, 1987); i.e.

$$\tau_\mathrm{b} = A_\mathrm{b}^{-1/m} N^p |\boldsymbol{v}_\mathrm{b}|^{1/m-1} \boldsymbol{v}_\mathrm{b}\,, \tag{1}$$

where τ_b is the basal shear stress, v_b is the basal sliding velocity, A_b is a spatially varying basal sliding coefficient, and N is the effective pressure at the base. Values of exponents m and p are generally within the range of 1–3, although higher values for m, leading to a more plastic behaviour, are also found (Gillet-Chaulet et al., 2016; Brondex et al., 2019). Values for A_b are obtained through a nudging method in which the modelled ice sheet is run in a steady state and slip coefficients A_b are adjusted to minimize the difference between modelled and observed ice thickness (Pollard and DeConto, 2012b; Pattyn, 2017). Subglacial hydrology generally enters Eq. (1) through the effective pressure N, which makes it part of the nudging scheme mentioned above.

At the ocean boundary, a grounding-line flux condition is employed (Pollard and DeConto, 2012b; Pattyn, 2017) in line with a Weertman sliding law (Schoof, 2007). However, such a flux condition is only valid when $p = 0$, as the flux condition is independent of effective pressure N. However, it is also valid for $p > 0$ as long as $N > 0$, as N then intrinsically makes part of the sliding pre-factor. In our experiments, we found the effective pressure is always non-zero at and in the vicinity of the grounding line. We will discuss the effect of $N = 0$ more in depth in the Discussion section.

2.1 Effective pressure at the ice sheet base

There are different ways of representing the effective pressure at the base of an ice sheet that are applied in ice sheet models. The effective pressure N is defined as the ice overburden pressure p_o, i.e. the downward force due to the weight of overlying ice, minus the subglacial water pressure (p_w):

$$N = p_\mathrm{o} - p_\mathrm{w} = \rho_\mathrm{i} g h - p_\mathrm{w}\,, \tag{2}$$

where ρ_i is the ice density, g is the gravitational acceleration, and h is the ice thickness. Values for all employed constants are provided in Table 1. In the following sections, we describe in more detail how the effective pressure N is de-

Table 1. List of constants and parameters used.

Symbol	Description	Units	Value
C_c	Till compressibility		0.12
C_t	Till drainage rate	$mm\,a^{-1}$	1
d_w^0	Maximum limit of subglacial water film thickness	m	15×10^{-3}
δ	Fraction of ice overburden pressure		0.02
e_0	Reference value of the sediment void ratio		0.69
ϕ_0	Water flux limit	$m^2\,a^{-1}$	10^5
g	Gravitational acceleration	$m\,s^{-2}$	9.81
m	Exponent in basal sliding law		1–5
μ	Water viscosity	Pa s	1.8×10^{-3}
N_0	Reference value of the effective basal pressure	Pa	1000
p	Exponent of the effective pressure		0–1
ρ_i	Ice density	$kg\,m^{-3}$	917
ρ_s	Ocean water density	$kg\,m^{-3}$	1027
ρ_w	Water density	$kg\,m^{-3}$	1000
W_{max}	Maximum saturated till layer thickness	m	2

termined in space and time, either directly or by determining the subglacial water pressure p_w.

2.1.1 Height above buoyancy (HAB)

A simple way to determine subglacial water pressure p_w is to link it directly to the depth of the bed below sea level (Van der Veen, 1987; Tsai et al., 2015; Martin et al., 2011; Winkelmann et al., 2011) so that high water pressure occurs in the deep subglacial basins and near the grounding line (Fig. 1). The subglacial water pressure at the base may then be approximated by

$$p_w = -P_w \rho_s g\,(b - z_{sl})\,, \tag{3}$$

where P_w is a fixed fraction of the overburden pressure, ρ_s is the density of seawater, b is the bedrock elevation, and z_{sl} is the local sea level height. Equation (3) is valid for $b - z_{sl} < 0$; otherwise $p_w = 0$. By definition, $p_w = \rho_i g h$ at the grounding line and underneath floating ice shelves, so the effective pressure becomes zero (or close to zero when modulated by the value of P_w). This means that only marine-terminating parts of the ice sheet are impacted by the subglacial water. According to Lüthi et al. (2002), the pore water pressure, i.e. the pressure of the subglacial water mixed with the solid part of the till, represents a fraction slightly smaller than 100 % of the ice overburden pressure. Bueler and Brown (2009) consider the pore water pressure locally at most a fixed fraction (P_w = 95 %) of the ice overburden pressure $\rho_i g h$. The fraction varies among different studies, i.e. 96 % (Martin et al., 2011; Winkelmann et al., 2011), 97 % (van Pelt and Oerlemans, 2012), and 99 % (Gandy et al., 2019). Here, we fixed $P_w = 0.96$. The use of HAB is probably the most common representation of subglacial water pressure in large-scale Antarctic ice sheet models, and the value of P_w prevents the effective pressure from becoming zero when the flotation criterion is reached (e.g. at the grounding line) to avoid numerical instabilities.

2.1.2 Subglacial water depth (SWD)

Subglacial water flow can be introduced following the method of Le Brocq et al. (2009) based on a single drainage element type to describe the morphology of the drainage system, i.e. a Weertman-type water film (Weertman, 1972; Walder, 1982; Weertman and Birchfield, 1982). The model assumes that water flows in a thin film of water of the order of 10^{-3} m thickness. The evolution of the water film depth d_w is given by

$$\frac{\partial d_w}{\partial t} = M - \nabla \cdot (\boldsymbol{u}_w d_w)\,, \tag{4}$$

where M is the basal melt rate (positive for melting) underneath the grounded ice sheet (Fig. 1) and $\boldsymbol{u}_w$ is the depth-averaged water film velocity, calculated using a theoretical treatment of laminar flow between two parallel plates, driven by differences in the water pressure (Weertman, 1966):

$$\boldsymbol{u}_w = \frac{d_w^2}{12\mu} \nabla \Phi\,, \tag{5}$$

where μ is the viscosity of water and Φ is the hydraulic potential. The hydraulic potential represents the total mechanical energy per unit volume of water required to drive water flow and is a function of the elevation potential and the water pressure (Le Brocq et al., 2009); i.e.

$$\Phi = \rho_w g b + p_w = \rho_w g b + \rho_i g h - N\,. \tag{6}$$

The water pressure, p_w, is a function of the ice overburden pressure and the effective pressure N. In a distributed system

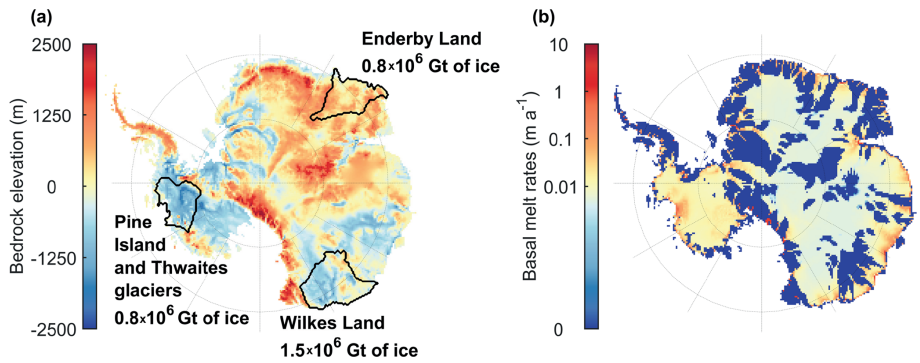

Figure 1. Bedrock elevation (m) based on BedMachine data (Morlighem et al., 2020) **(a)** and calculated basal melt rates ($\mathrm{m\,a^{-1}}$) with the ice sheet model **(b)**. Selected drainage basins shown are discussed in Sect. 4.2.

(opposite to the channelized system; Flowers, 2015), however, the water pressure will be close to, if not at, the overburden pressure. As a result, a simplification can be made to Eq. (6), assuming N to be zero (Budd and Jenssen, 1987; Alley, 1989). The assumption that N is zero simplifies the calculation of the hydraulic potential surface by removing the need to calculate the water pressure. With this simplification, the gradient of the potential surface is written as

$$\nabla\Phi = \rho_\mathrm{i} g \nabla h_\mathrm{s} + (\rho_\mathrm{w} - \rho_\mathrm{i}) g \nabla b\,. \tag{7}$$

Taking $\partial d_\mathrm{w}/\partial t = 0$ in Eq. (4) (steady-state approach), it is possible to use a flux balance approach to calculate the steady-state water depth in a similar way to balance velocity calculations (Budd and Warner, 1996; Le Brocq et al., 2006). The balance approach requires the outgoing flux in any given grid cell to be equal to the incoming water flux plus the local melt rate within the cell. The routing direction of the subglacial water is given by the hydraulic potential gradient $\nabla\Phi$. The water depth is then obtained from the outgoing water flux Q_l; i.e.

$$d_\mathrm{w} = \left(\frac{12\mu Q_l}{|\nabla\Phi|}\right)^{\frac{1}{3}}. \tag{8}$$

Q_l is calculated as the incoming flux plus the basal melting rate corrected for the unit width of the cell or the subglacial water speed multiplied by the subglacial water thickness. The same method is used for determining balance fluxes of ice in Le Brocq et al. (2006). Subglacial water thickness is then related to subglacial water pressure through

$$p_\mathrm{w} = P_\mathrm{w} \rho g h \left(\frac{d_\mathrm{w}}{d_\mathrm{w}^0}\right), \tag{9}$$

where $d_\mathrm{w}^0 = 0.015\,\mathrm{m}$ is a limit value to the subglacial water thickness.

2.1.3 Sliding related to water flux (SWF)

Alternatively, Goeller et al. (2013) propose introducing a simple physically plausible correlation of the basal sliding coefficient and the subglacial water flux ϕ; i.e.

$$A_\mathrm{b} = A_\mathrm{o} \exp\left(\frac{\phi}{\phi_0}\right), \tag{10}$$

where ϕ_0 is a limit factor on the subglacial water flux (Goeller et al., 2013) and A_o the initial value of A_b, obtained through the nudging method. A similar approach has been followed by Pattyn et al. (2005). The approach considers that basal sliding increases when the water flux beneath the ice sheet increases, which is however more intuitive than physically sound as the water flux generally increases towards the grounding line, hence leading to the highest sliding velocities at the grounding line. Since the subglacial hydrology enters through the basal sliding coefficient, the effective pressure N is not considered in the sliding law.

2.1.4 Effective pressure in till (TIL)

Bueler and Brown (2009) employ an effective thickness of stored liquid water at the base of the ice column. This layer of thickness W is used to estimate the subglacial water pressure reduced to the pore water pressure according to

$$p_\mathrm{w} = P_\mathrm{w} \rho_\mathrm{i} g h \frac{W}{W_\mathrm{max}}, \tag{11}$$

where W_max is the maximum saturated till thickness, fixed at 2 m, which has an impact on the till weakening by pressurized water. This value is taken from Bueler and Brown (2009) and van Pelt and Oerlemans (2012) and is used in the standard Parallel Ice Sheet Model (PISM). A fixed fraction of ice overburden equal to one implies an effective pressure and consequently a yield stress equal to zero in the case of full till saturation (Eq. 1; van Pelt and Oerlemans, 2012). An alternative approach consists of deriving the effective pressure in the case of a deformable bed composed of permeable till. The effective pressure, N, in Eq. (2) is expressed as a function of the sediment void ratio, e, due to the changing water content in the till (van der Wel et al., 2013; Bougamont et al., 2014); i.e.

$$N = N_0 \times 10^{-(e-e_0)/C_\mathrm{c}}, \tag{12}$$

Table 2. Summary of the subglacial models.

Type	Description	Eq.
NON	$p = 0$: no effective pressure	
HAB	p_w from marine basin depth	(3)
SWD	p_w from subglacial water depth	(9)
SWF	A_b from subglacial water flux	(10)
TIL	N from saturated till	(14)

where e_0 is the void ratio at a reference effective pressure N_0 and C_c is the dimensionless coefficient of till compressibility (Tulaczyk et al., 2000). Bueler and van Pelt (2015) propose employing Eq. (12) in a hydrological model of subglacial water drainage within an active layer of the till, W. As the water in till pore spaces is much less mobile than that in the linked-cavity system because of the very low hydraulic conductivity of till, an evolution equation for W without horizontal transport can be written (Bueler and van Pelt, 2015):

$$\frac{\partial W}{\partial t} = M - C_t. \tag{13}$$

Here, C_t is a fixed rate that makes the till gradually drain in the absence of water input; we choose C_t to be $1\,\mathrm{mm\,a^{-1}}$ (Pattyn et al., 2005; Bueler and van Pelt, 2015), which is small compared to typical values of subglacial melt. We constrain the layer thickness by $0 \le W \le W_{max}$. The effective pressure N is then written as the following function of W (Bueler and van Pelt, 2015),

$$N = N_0 \left(\frac{\delta p_o}{N_0}\right)^s 10^{\left(\frac{e_0}{C_c}\right)(1-s)}, \tag{14}$$

where $s = W/W_{max}$ and is bounded by $N = \min\{p_o, N\}$ and δp_o is the lower bound on N, taken as a fraction δ of the ice overburden pressure p_o. The value of W_{max} is taken from Bueler and Brown (2009) and van Pelt and Oerlemans (2012) and is used in the standard PISM.

3 Experimental setup

The experimental setup (Fig. 2) starts from a steady-state ice sheet configuration for which a field of basal sliding coefficients A_b are obtained through a nudging method (Pollard and DeConto, 2012a; Pattyn, 2017). To initialize the ice sheet model, we optimized the basal sliding coefficients A_b to fit the modelled ice sheet geometry to the observed one for four exponents of the sliding law (Eq. 1), ranging from viscous sliding $m = 1$ to near-plastic sliding $m = 5$ and with $p = 1$ to express the effective pressure for each of the subglacial models HAB, SWD, SWF, and TIL (Table 2). For each of the sliding exponents, a control run (NON) was established for $p = 0$, where the effective pressure is disregarded so that Eq. (1) represents a Weertman sliding law.

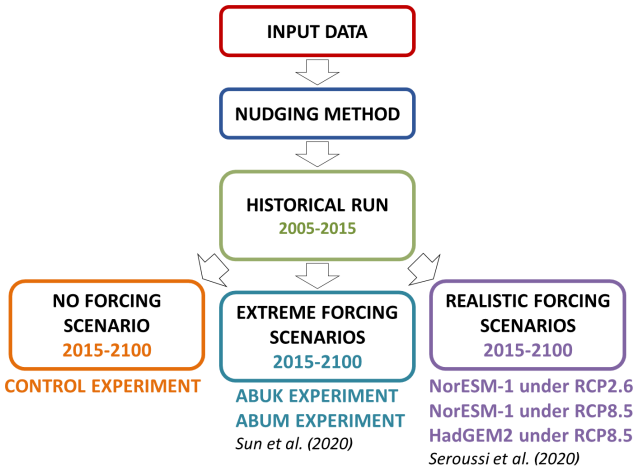

Figure 2. Flow chart of the experimental setup.

A short historical run was performed for a period of 10 years (Fig. 2), forced with conditions of temperature and sub-shelf melt representative of the conditions estimated between 2005 and 2015 (Seroussi et al., 2020), and thus also serves as a relaxation run. Starting from the historical run, we performed three types of experiments: (i) a control experiment for which climate forcing was not considered (prolongation of the historical run), (ii) the ABUMIP experiments where ice shelves were either removed or subject to very high sub-shelf melt rates (Sun et al., 2020), and (iii) climate forcing scenarios for different Representative Concentration Pathways (RCPs) and for two different climate models (Seroussi et al., 2020). All runs started at the end of the historical run (2015 CE) and ran until the year 2100. The ISMIP6 set enables us to gauge the sensitivity under realistic climate scenarios, while the ABUMIP set allows us to test the sensitivity of the sliding laws and subglacial models under extreme high forcing and ice sheet collapse. For the historical, control, and ISMIP6 runs, sub-shelf melting was determined through the ISMIP6 parameterization based on ocean temperature and salinity for different basins, according to the method explained in Jourdain et al. (2020) and Seroussi et al. (2020).

3.1 Historical run

Figure 3 displays the main characteristics of the different subglacial model approaches for the grounded part of the Antarctic ice sheet after the historical run. The HAB subglacial water pressure, which is related to the bed topography (Fig. 1), reaches the highest values near the grounding line and in the deepest parts of the marine basins of the ice sheet. These high values are prevalent underneath the West Antarctic ice sheet. Water pressure due to subglacial water depths (SWD model) is highest where ice flow is concentrated, i.e. in the major ice streams draining the Antarctic ice sheet, and has non-zero values for the areas where subglacial water is

present (where the ice reaches the pressure melting point at the base). A similar pattern is obtained for the SWF model, with stronger concentrations of water fluxes in the downstream parts of the ice streams, especially near the grounding lines. Finally, the TIL model exhibits a quasi-constant field of very low effective pressure N for the areas that are at the pressure melting point. The main reason for this particular behaviour is that the till layer – due to generally constant basal temperature conditions – is saturated across these areas, leading to an effective pressure corresponding to saturated till (Fig. 4).

3.2 ABUMIP experiments

The ABUMIP experiments (Sun et al., 2020) present an idealized case for gauging the sensitivity of sliding laws when extreme forcing is applied. The first experiment (ABUK) consists of removing instantaneously all the ice shelves surrounding the ice sheet at the start of the run and removing any newly formed floating ice instantaneously afterwards (so-called "float-kill"). In other words, at all times, the calving flux is assumed to be larger than the flux across the grounding line to prohibit regrowth of the shelves. The second experiment (ABUM) is similar, but instead of removing the ice shelves, a constant high value of sub-shelf melt ($400\,\mathrm{m\,a^{-1}}$) is applied to all ice shelves.

The ABUMIP experiments previously showed a tendency for increased model sensitivity to the power of the sliding law, leading to more mass loss for a higher power in power-law sliding (Sun et al., 2020). Here, we make a further comparison with different hydrologies for different powers in the Weertman–Budd sliding law.

3.3 ISMIP6 experiments

For this set of experiments, we applied three different ISMIP6 forcings in surface mass balance and ocean temperature starting from the historical run (Nowicki et al., 2016; Seroussi et al., 2020). These are the NorESM1-M atmosphere–ocean general circulation model (AOGCM) for two climate scenarios (RCP2.6 and RCP8.5) and the HadGEM2-ES AOGCM for RCP8.5. The latter was chosen for its higher mass loss response of the Antarctic ice sheet (Seroussi et al., 2020). Compared to the ABUMIP experiments, these tests allow for a more realistic future behaviour of the ice sheet, as well as a more in-depth analysis of the subglacial hydrological behaviour for selected basins and bed types.

4 Results

4.1 ABUMIP experiments

A sudden and sustained loss of ice shelves according to the ABUK experiment (Fig. 5) leads to Antarctic mass loss of between 2 and 6.5 m s.l.e. by the end of the century. Mass loss increases with increasing values of m in Eq. (1). The effect of subglacial hydrology modulates this response for each of the values of m and is of the order of 0.5 m around the result of the NON experiment for each value of m (Fig. 5).

Incorporating hydrology into the model generally leads to a higher sensitivity, where SWD and HAB show a higher mass loss due to the applied forcing (loss of ice shelves). The subglacial till model (TIL) does not add significant change in the response of the ice sheet compared to the absence of basal hydrological coupling (NON). This may be explained by the rather constant value of effective pressure N for TIL across the basal temperate zones of the Antarctic ice sheet (Fig. 3) where mass loss occurs. Higher variability in N (or p_{w}), especially lower values of N within the fast-flowing ice streams, leads to a faster grounding-line retreat.

Similar characteristics are shown for the ABUM experiment, where an extreme high sub-shelf melt rate was imposed (Fig. 5). Here, Antarctic ice mass loss lies slightly lower (between 2 and 5 m by 2100). Again, subglacial hydrological coupling modulates mass loss for different power in the sliding law, similarly to what is observed for the ABUK experiment.

4.2 ISMIP6 experiments

Results of the ISMIP6 experiments with the NorESM1-M AOGCM forcing are displayed in Figs. 6 and 7 for RCP2.6 and RCP8.5, respectively. To gauge the sensitivity of the different subglacial hydrologies, we subtracted the mean model drift from the control run for each of the experiment series ($m = 1$–5) from the time series of the forcing experiments. The drift in the control experiment was observed to increase linearly in time. This way, each of the subglacial approaches has the same model drift correction.

For a low-forcing scenario (RCP2.6), model runs without subglacial hydrology lead to minimal ice volume change (in some cases a slight mass change; Fig. 6). Coupling with subglacial hydrology again modulates this signal, characterized by a sensitivity similar to the ABUMIP experiments, where HAB generally leads to higher mass losses (between 3 and 9 cm by 2100). A similar response is also observed for the high-forcing scenario (RCP8.5), making the contribution of the Antarctic ice sheet to sea level change at the end of the century rather independent of forcing (Fig. 7). Similar conclusions were also obtained in a multi-model analysis using the same forcing (Seroussi et al., 2020; Edwards et al., 2021). More striking, however, is that the obvious sensitivity to the power of the sliding law m is absent from both low- and high-

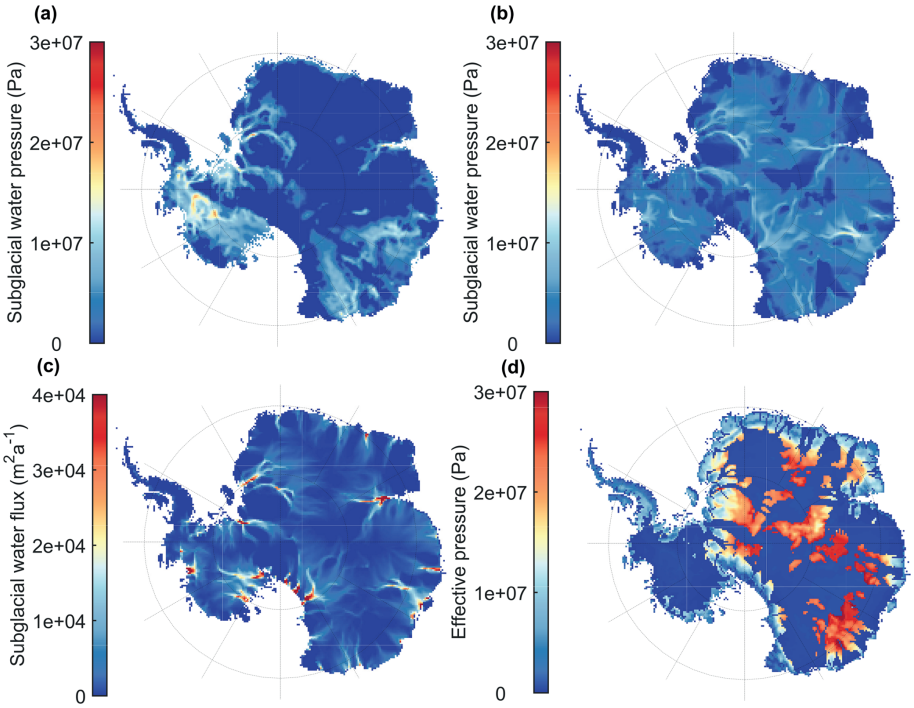

Figure 3. Steady-state subglacial characteristics for the Antarctic ice sheet according to the different subglacial models: **(a)** HAB subglacial water pressure (Pa); **(b)** SWD subglacial water pressure (Pa); **(c)** SWF subglacial water flux ($m^2\,a^{-1}$); **(d)** TIL effective pressure (Pa).

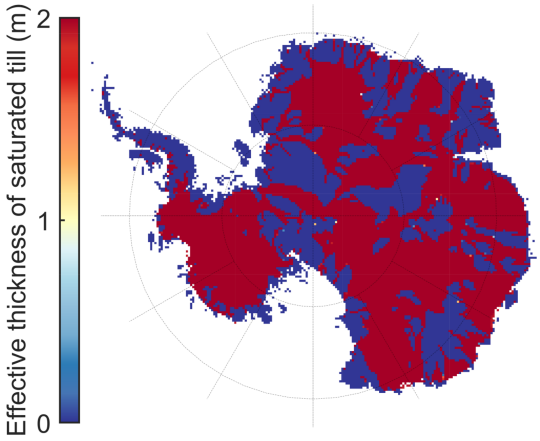

Figure 4. Effective thickness of saturated till (maximum value fixed at 2 m) for the TIL experiment.

forcing scenarios and that the variability in response is dominated by hydrological coupling instead of the plasticity of the power law.

Similarly to the results from the ISMIP6 model intercomparison, to which the f.ETISh model contributed, NorESM forcing according to RCP8.5 does not significantly differ from the low-forcing scenario (Fig. 7) in terms of simulated ice volume above floatation by 2100 (Seroussi et al., 2020). While the values of mass change are slightly larger, the modulation for different subglacial hydrologies is larger as well.

The HadGEM2 forcing according to RCP8.5 shows a more distinct positive sea level contribution across the different ice sheet models within ISMIP6 (Seroussi et al., 2020). Overall, HadGEM2 forcing leads to higher mass losses, in line with the ISMIP6 results (Fig. 8). In terms of hydrological coupling, HAB is still the most important contributor to ice mass loss, and the variability in sea level contribution between the different hydrological coupling schemes is also comparable to NorESM.

A more in-depth analysis of the HadGEM2 RCP8.5 results is made for selected drainage basins, each with particular subglacial characteristics, i.e. Pine Island and Thwaites glaciers, Wilkes Land, and Enderby Land (Fig. 1). Pine Island and Thwaites glaciers are typical marine basins of the West Antarctic ice sheet where most of the current ice mass loss is situated; Wilkes Land is a subglacial basin of the East Antarctic ice sheet (EAIS) with the potential for instability (Mengel and Levermann, 2014), and Enderby Land is part of the East Antarctic ice sheet where the bed is mostly lying above sea level and where the contact with the ocean is limited (continental ice sheet). All basins contain a more or less comparable ice volume (between 0.8 and 1.5×10^6 Gt).

The highest mass loss occurs in the marine basins of Pine Island and Thwaites glaciers (Fig. 9), followed by Wilkes basin. Both marine basins have in general the highest response for HAB. Viscous sliding ($m = 1$) has the lowest sensitivity, but higher plasticity of the sliding law does not necessarily result in a higher sensitivity. For instance, Pine Is-

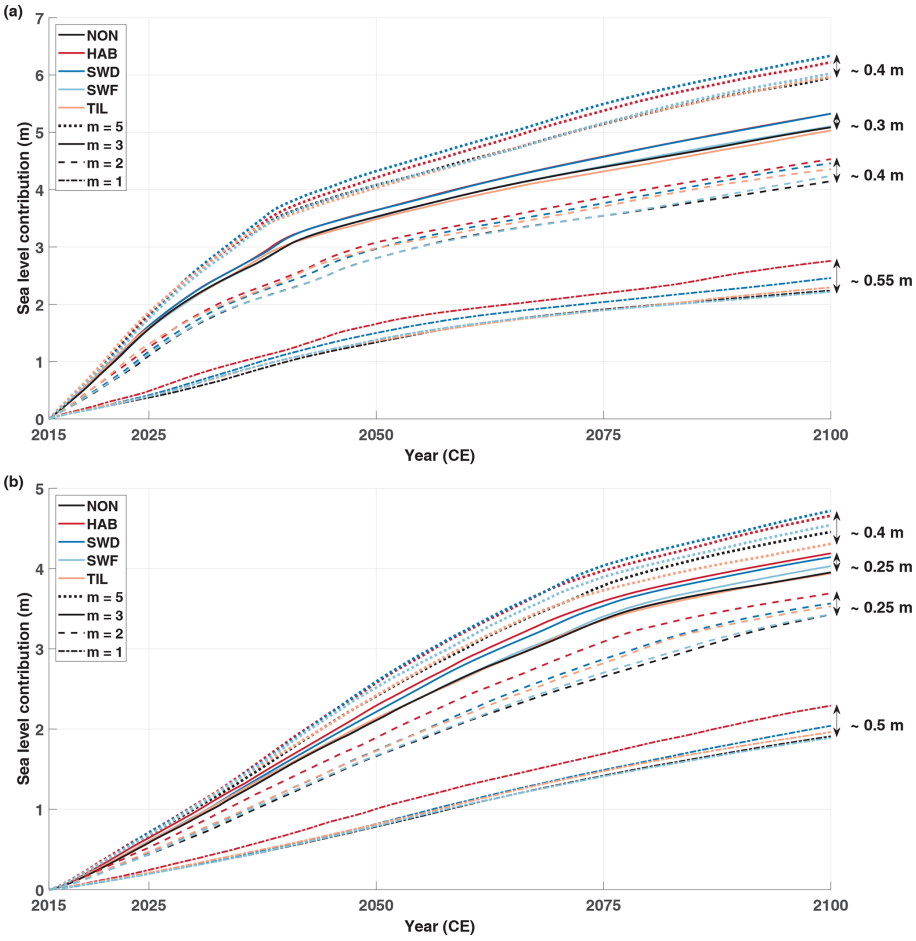

Figure 5. Sea level contribution from the Antarctic ice sheet until 2100 for ABUK **(a)** and ABUM **(b)** experiments. Line colours represent the different subglacial models (Table 2), and the different line styles express the exponent value of the basal sliding law.

land and Thwaites glaciers exhibit the highest sensitivity for $m = 2$, while for Wilkes Land this is for $m = 5$. The complexity in response is therefore attributable to other factors at play, such as increased accumulation rates and the relatively weak ocean forcing from the HadGEM2 model over this period. The TIL model seems overall more responsive for a higher degree of plasticity of the sliding law. The continental basin (Enderby Land) has only a limited contact with the ocean. Not only are the relative contributions to sea level very minor, but any tendency as is seen for the marine basins is also lacking. The TIL model for Enderby Land is also less sensitive because of the lack of saturated till in this basin. In summary, on a basin level, subglacial hydrology has a more uncertain effect on the response of the ice sheet to forcing from global climate models.

5 Discussion

From the above experiments it can be seen that in general, subglacial hydrology increases the sensitivity in response to forcing compared to models where subglacial hydrology is ignored. The uncertainty raised by subglacial hydrology models is comparable to that between different ice sheet models under RCP scenarios (Seroussi et al., 2020). With non-linear basal sliding laws, an evolving subglacial hydrological system increases the sea level contribution of Antarctica under different RCP scenarios (Figs. 6–8). This is especially the case for the common HAB model (Van der Veen, 1987; Martin et al., 2011; Winkelmann et al., 2011; Tsai et al., 2015), where the effective pressure at the base of the ice decreases with bed depth and is closest to zero in deep marine basins and near the grounding line (Fig. 3). The SWD model also exhibits a relatively high sensitivity, especially in the ABUK and ABUM experiments. Here, values of effective pressure are generally higher throughout the basins, but low values are concentrated in the ice streams and especially close to the grounding line, where they have an impact on the grounding-line sensitivity. All other subglacial models are characterized by higher values of N, which leads to a reduced sensitivity.

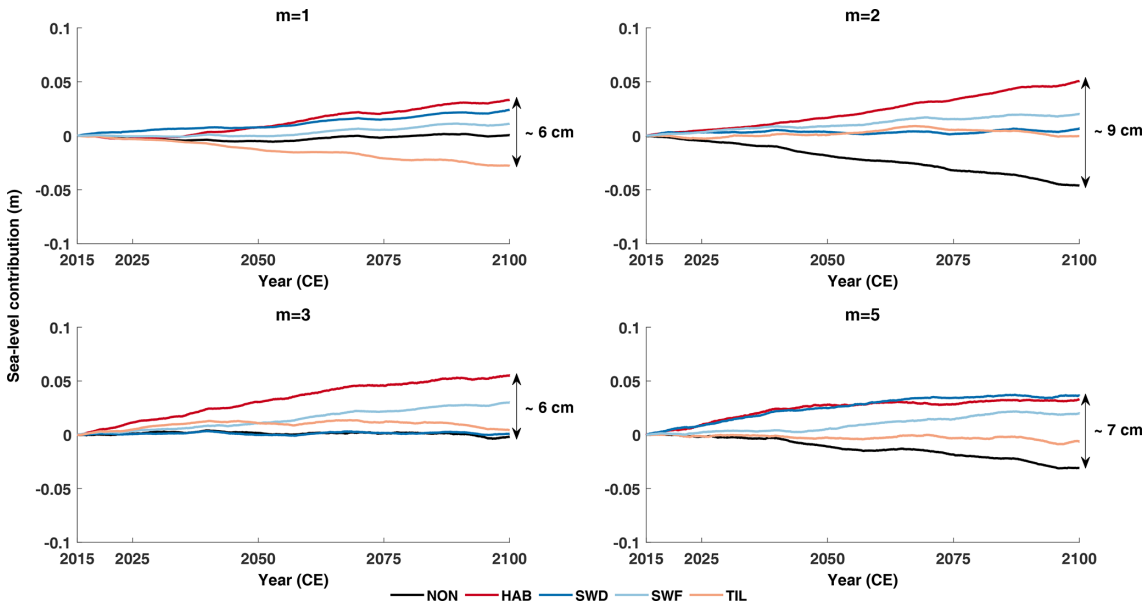

Figure 6. Sea level contribution from the Antarctic ice sheet until 2100 following NorESM1 in the RCP2.6 scenario. Each graph gives the results for one exponent of the basal sliding law, and line colours represent the different subglacial models (Table 2).

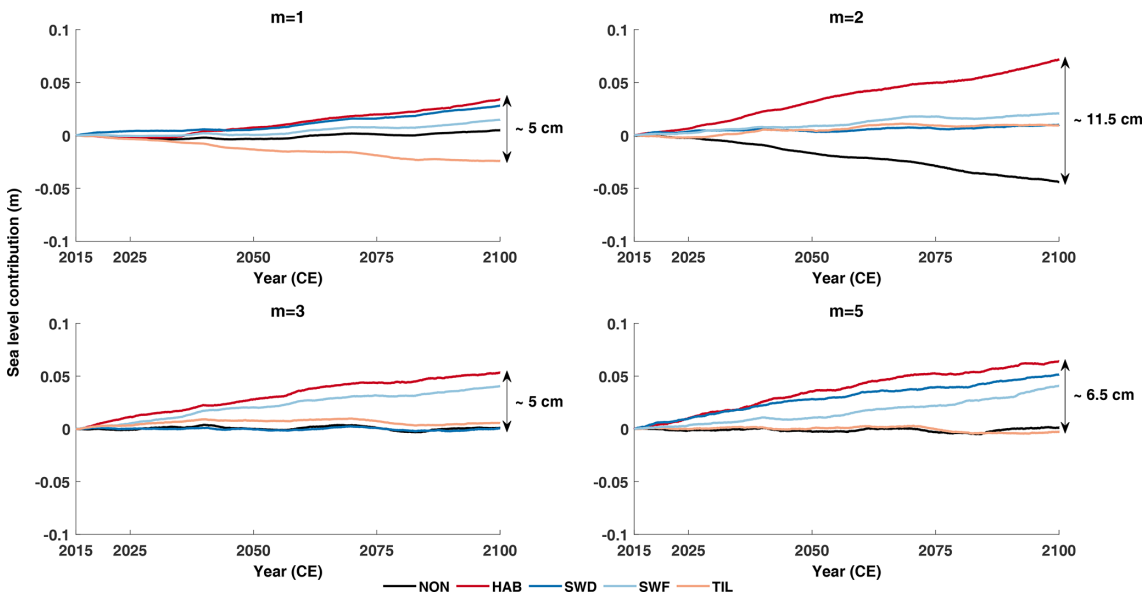

Figure 7. Sea level contribution from the Antarctic ice sheet until 2100 following NorESM1 in the RCP8.5 scenario. Each graph gives the results for one exponent of the basal sliding law, and line colours represent the different subglacial models (Table 2).

A clear relationship between ice sheet sensitivity to forcing and the power in the basal sliding law is found for the ABUMIP experiments, leading to a higher sensitivity to climate forcing for more plastic sliding laws (Sun et al., 2020). Such a clear relationship is lacking in the ISMIP6 forcing experiments. This is probably due to a more complex interaction between the ice sheet and the forcing, as increased temperatures lead not only to more sub-shelf melt but also to increased surface accumulation (Seroussi et al., 2020). The latter may therefore offset mass loss due to grounding-line retreat in certain Antarctic drainage basins.

For the different representations of the effective pressure N in this paper, the pattern of the optimized slip coefficients A_b is rather similar, although their absolute values may differ, especially for the TIL model (Supplement Figs. S1 and S2). Overall, the highest values of A_b are found on the Siple Coast, in the Amundsen Sea area, and in the Recovery basin, where the fastest ice flow also occurs. Low values of effective

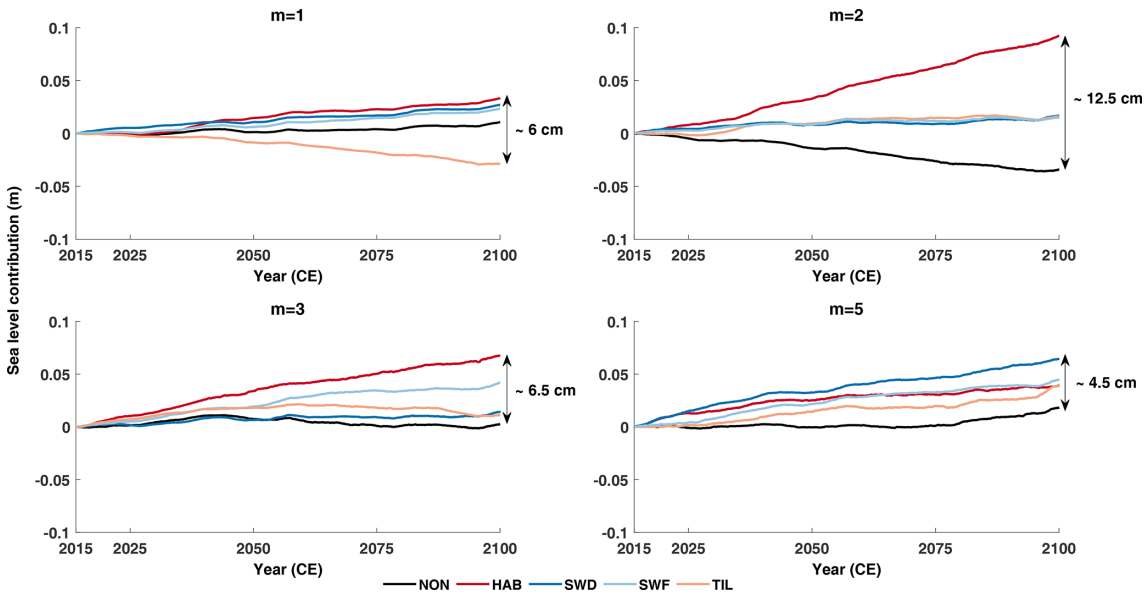

Figure 8. Sea level contribution from the Antarctic ice sheet until 2100 following HadGEM2 in the RCP8.5 scenario. Each graph gives the results for one exponent of the basal sliding law, and line colours represent the different subglacial models (Table 2).

pressure N in these areas only partially alter the value of the optimized slip coefficients but do not substantially change the pattern of A_b. The same pattern is also obtained for different values of the power in the power law m, demonstrating that the optimization scheme is rather robust. The use of a low-pass filter for the regularization to avoid overfitting also helps the robustness of the method (Pattyn, 2017).

In principle, the effective pressure becomes zero at the grounding line, as the water pressure equals the ice overburden pressure (Tsai et al., 2015). For ice shelves, the effective pressure equals zero by definition. However, in large-scale models, this condition is never really met, as the grounding line is a large grid cell and not exactly a boundary, and limiting factors are introduced to avoid $N = 0$, which could lead to numerical instabilities. For the Coulomb-limiting case where N becomes zero at the grounding line, Tsai et al. (2015) found that the grounding-line ice flux depends more strongly on the floating ice thickness compared to the Weertman sliding case and that the ice sheet may ground stably in shallower water. This implies that smaller perturbations are required to move the grounding line into regions of retrograde bed slope compared to a power-law rheology, which makes ice sheets more sensitive to climate perturbations.

In our ice sheet model, a flux condition is employed at the grounding line, corresponding to power-law sliding. This flux condition is imposed as an internal boundary condition following the implementation by Pollard and DeConto (2012a, b) based on Schoof (2007). This implementation has been shown to reproduce the migration of the grounding line and correctly reproduce steady-state grounding-line positions for coarse-resolution shallow-shelf approximation (SSA) and hybrid SSA–shallow-ice approximation (SIA) models (Pattyn et al., 2013; Pattyn and Durand, 2013). Tsai et al. (2015) derived a similar flux condition for the Coulomb friction case where $N = 0$ at the grounding line. We also implemented this particular case for a linear Coulomb sliding law (Bueler and van Pelt, 2015); i.e. $\tau_b = CN\boldsymbol{u}$, where C is a friction coefficient related to subglacial till properties. Such a friction law is very similar to the Weertman sliding law with $m = 1$. For this linear case, the grounding-line flux is equivalent to $q_g \sim h_g^{n+2}$, compared to $q_g \sim h_g^{2+n/2}$ for a linear sliding law following the derivation of Schoof (2007). We therefore expect a higher sensitivity of the grounding-line flux to ice thickness for the Coulomb law, which has been shown previously (Bulthuis et al., 2019; Sun et al., 2020). We obtain similar results for the ABUK and ABUM experiments, i.e. a significantly higher mass loss when the Tsai et al. (2015) grounding-line flux is applied. In all cases this leads to the complete collapse of the WAIS within a century and a consequent grounding-line retreat in some EAIS basins, such as the Wilkes basin (Fig. 10). However, the impact of the different hydrological models follows the same modulation as for the power-law cases, where the HAB model adds to the sensitivity of the grounding line due to lower effective pressures at the bed.

Only a limited number of subglacial models have been explored in this paper, and the processes on which they are based are relatively simple. These encompass sliding on hard and soft beds, through the presence of a water film (SWD, SWF), through elementary till mechanics based on subglacial meltwater saturating the underlying till layer (TIL), or by reduced coupling of the ice with the bed through lower effective pressure in grounding zones (HAB). Especially the

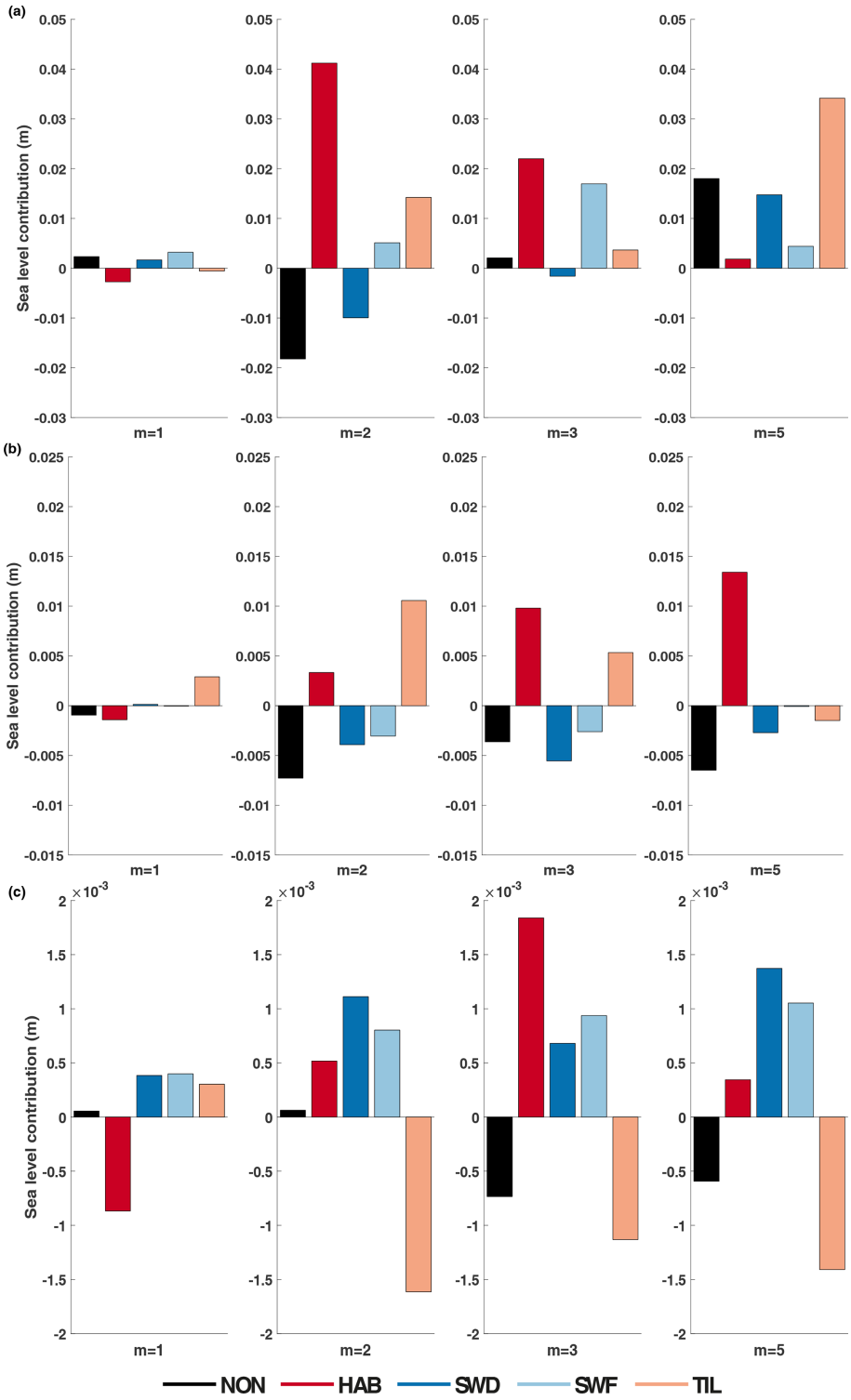

Figure 9. Sea level contribution according to HadGEM2 RCP8.5 for different basins and different values of m in the sliding law and subglacial hydrology: Pine Island and Thwaites glaciers **(a)**, Wilkes Land **(b)**, and Enderby Land **(c)**. Colour bars represent the different subglacial models (Table 2).

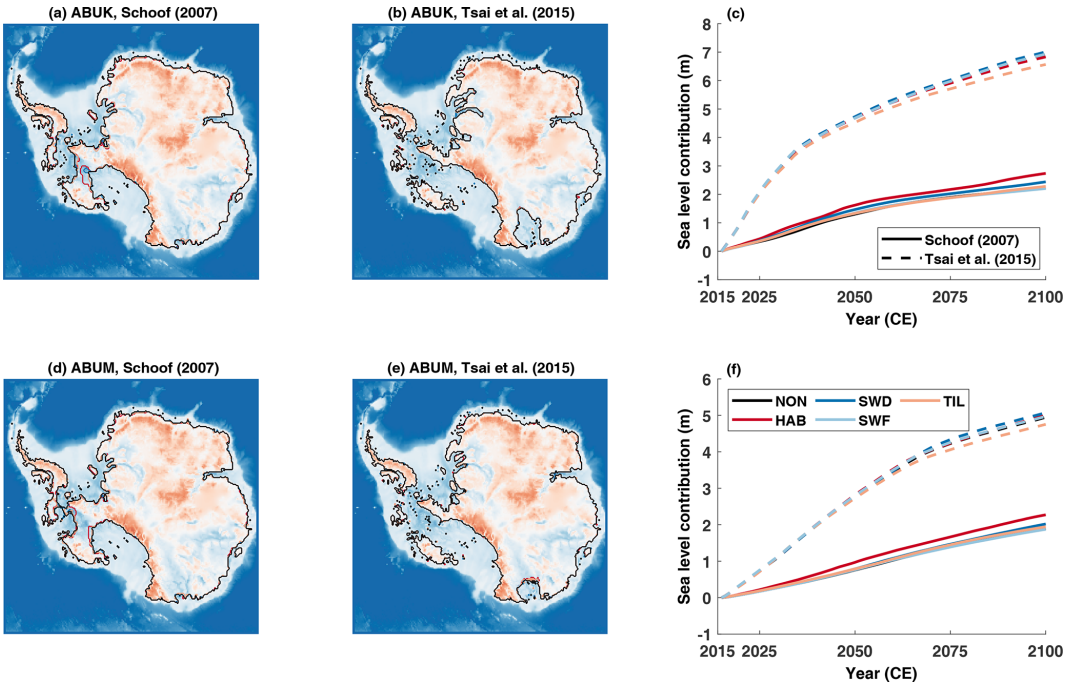

Figure 10. Grounding-line positions at 2100 CE for ABUK and ABUM experiments for both grounding-line flux conditions **(a, b, d, e)** and associated mass loss over the same period (**c**: ABUK, **f**: ABUM). In these experiments the exponent of the sliding law m is equal to 1. Line colours represent the different subglacial models (Table 2); solid lines represent a grounding-line flux parameterization due to Schoof (2007) (standard runs) and dashed lines one due to Tsai et al. (2015). Grounding-line positions in the left and middle panels are largely overlapping.

latter is the simplest of all, but it also leads to the highest sensitivity in the different forcing experiments that are presented here. Its validity is limited to the grounding zone, where it represents the intrusion of seawater reducing the effective pressure in this area. Such a process may well occur tens of kilometres upstream of the grounding line (Golledge et al., 2015; Robel et al., 2022). However, its applicability further inland across submarine basins can be questioned.

Limits to the models are also due to considering a stable hydrological system. Commonly, a distinction is made between channelized (efficient) and sheetlike (inefficient or distributed) drainage systems. Here, only the sheetlike system has been considered, albeit as a stable system (steady state), thereby intrinsically preventing unstable behaviour, such as the formation of cavities leading to ice sheet accelerations (Schoof, 2010). This may in part explain the weak sensitivity of SWD and SWF models to the applied forcing.

The evolution of the till-stored water layer thickness (Bueler and Brown, 2009; Bueler and van Pelt, 2015) also has some limitations in the way it is presented here. The evolution of the till layer thickness (Eq. 13) is limited by a maximum thickness $W_{\max}$. For the timescales considered here, the evolution of the subglacial temperate areas is rather constant, leading to a more or less temporally constant distribution of saturated till thickness in time (Fig. 4). A retreating grounding line will therefore not experience changing basal conditions as the marine basins are already at saturation.

Finally, the SWF model, which is also based on the balanced water layer concept (Le Brocq et al., 2009; Goeller et al., 2013), employs a simple, but physically plausible, correlation of the sliding rate to the subglacial water flux via an exponential function (Eq. 10). This functional relationship increases basal sliding with increasing basal water flux compared to a baseline water flux and basal sliding rate. While the approach is probably an oversimplified way of linking both systems, its effect on the ice sheet behaviour remains rather limited. In most cases it behaves in a very similar way to if hydrological coupling were omitted.

6 Conclusions

We investigated the role of subglacial hydrology and till deformation on the behaviour of the Antarctic ice sheet using a large-scale ice sheet model. We considered both sliding over a hard bed with the presence of a thin water film and deformation of saturated till at the base of the ice sheet. Both effective pressure models were compared to other common representations of effective pressure in the literature. Our model results confirm that the power m in the power-law (Weertman–Budd) sliding law is the most controlling factor determining mass changes of the Antarctic ice sheet, as has been discussed and concluded elsewhere (Brondex et al., 2019; Bulthuis et al., 2019; Sun et al., 2020). Spatial vari-

ation in effective pressure N modulates basal sliding for a given value of the power-law exponent, where reduced effective pressure in the grounding zone generally increases the ice sheet sensitivity, especially for high-end scenarios, such as ABUMIP. This dependency is, however, less clear under realistic forcing scenarios (ISMIP6).

Overall, subglacial hydrological models that lead to low values of effective pressure in the grounding zone (such as HAB and SWD) increase ice sheet sensitivity to forcing. In the limit case, where the effective pressure equals zero at the grounding line (Tsai et al., 2015), sensitivity is largely increased and becomes less dependent on the type of sliding law.

Code and data availability. The f.ETISh model code can be downloaded from the PARASO source code package (https://doi.org/10.5281/zenodo.5337510, Pelletier et al., 2021) that belongs to Pelletier et al. (2022). All datasets used in this study are freely accessible through their original references. We employed BedMachine Antarctica version 2 (https://doi.org/10.5067/E1QL9HFQ7A8M, Morlighem, 2020). The ISMIP6 forcing datasets are available from the ISMIP6 website and data portal (https://www.climate-cryosphere.org/wiki/index.php?title=ISMIP6_wiki_page, ISMIP6 committee, 2022). All data and scripts for reproducing the figures in the paper are available on the online repository Zenodo (https://doi.org/10.5281/zenodo.7118690, Kazmierczak et al., 2022).

Supplement. The supplement related to this article is available online at: https://doi.org/10.5194/tc-16-4537-2022-supplement.

Author contributions. EK and FP designed the experimental setup and wrote the paper. All experiments were performed by EK with additional contributions from SS and VC. All authors contributed to the writing of the final manuscript.

Competing interests. The contact author has declared that none of the authors has any competing interests.

Disclaimer. Publisher's note: Copernicus Publications remains neutral with regard to jurisdictional claims in published maps and institutional affiliations.

Acknowledgements. This publication was supported by PROTECT. This project has received funding from the European Union's Horizon 2020 research and innovation programme under grant agreement no. 869304, PROTECT contribution number 33. Computational resources have been provided by the Consortium des Équipements de Calcul Intensif (CÉCI), funded by the Fonds de la Recherche Scientifique de Belgique (F.R.S.-FNRS) under grant no. 2.5020.11 and by the Walloon Region.

Financial support. This research has been supported by a scholarship of the Université libre de Bruxelles and partly by the European Union's Horizon 2020 research and innovation programme under grant agreement no. 869304.

Review statement. This paper was edited by Elisa Mantelli and reviewed by Samuel Cook and one anonymous referee.

References

Alley, R. B.: Water-Pressure Coupling of Sliding and Bed Deformation: I. Water System, J. Glaciol., 35, 108–118, 1989.

Alley, R. B., Anandakrishnan, S., Christianson, K., Horgan, H. J., Muto, A., Parizek, B. R., Pollard, D., and Walker, R. T.: Oceanic forcing of ice-sheet retreat: West Antarctica and more, Annu. Rev. Earth Planet. Sci., 43, 207–231, 2015.

Asay-Davis, X. S., Jourdain, N. C., and Nakayama, Y.: Developments in simulating and parameterizing interactions between the Southern Ocean and the Antarctic ice sheet, Current Climate Change Reports, 3, 316–329, 2017.

Beyer, S., Kleiner, T., Aizinger, V., Rückamp, M., and Humbert, A.: A confined–unconfined aquifer model for subglacial hydrology and its application to the Northeast Greenland Ice Stream, The Cryosphere, 12, 3931–3947, https://doi.org/10.5194/tc-12-3931-2018, 2018.

Bindschadler, R.: The importance of pressurized subglacial water in separation and sliding at the glacier bed, J. Glaciol., 29, 3–19, 1983.

Bougamont, M., Christoffersen, P., Hubbard, A. L., Fitzpatrick, A. A., Doyle, S. H., and Carter, S. P.: Sensitive response of the Greenland Ice Sheet to surface melt drainage over a soft bed, Nat. Commun., 5, 5052, https://doi.org/10.1038/ncomms6052, 2014.

Brinkerhoff, D. J., Meyer, C. R., Bueler, E., Truffer, M., and Bartholomaus, T. C.: Inversion of a glacier hydrology model, Ann. Glaciol., 57, 84–95, 2016.

Brondex, J., Gillet-Chaulet, F., and Gagliardini, O.: Sensitivity of centennial mass loss projections of the Amundsen basin to the friction law, The Cryosphere, 13, 177–195, https://doi.org/10.5194/tc-13-177-2019, 2019.

Budd, W., Keage, P., and Blundy, N.: Empirical studies of ice sliding, J. Glaciol., 23, 157–170, 1979.

Budd, W. F. and Jenssen, D.: Numerical Modelling of the Large-Scale Basal Water Flux under the West Antarctic Ice Sheet, in: Dynamics of the West Antarctic Ice Sheet, edited by: Van der Veen, C. and Oerlemans, J., pp. 293–320, Dordrecht, Kluwer Academic Publishers, 1987.

Budd, W. F. and Warner, R. C.: A Computer Scheme for Rapid Calculations of Balance-Flux Distributions, Ann. Glaciol., 23, 21–27, 1996.

Bueler, E. and Brown, J.: Shallow shelf approximation as a "sliding law" in a thermomechanically coupled ice sheet model, J. Geophys. Res.-Earth Surface, 114, f03008, https://doi.org/10.1029/2008JF001179, 2009.

Bueler, E. and van Pelt, W.: Mass-conserving subglacial hydrology in the Parallel Ice Sheet Model version 0.6, Geosci. Model Dev., 8, 1613–1635, https://doi.org/10.5194/gmd-8-1613-2015, 2015.

Bulthuis, K., Arnst, M., Sun, S., and Pattyn, F.: Uncertainty quantification of the multi-centennial response of the Antarctic ice sheet to climate change, The Cryosphere, 13, 1349–1380, https://doi.org/10.5194/tc-13-1349-2019, 2019.

Clarke, G. K. C.: Subglacial Processes, Ann. Rev. Earth Planet. Sci., 33, 247–276, 2005.

Cuffey, K. and Paterson, W. S. B.: The Physics of Glaciers. 4th ed, Elsevier, New York, 2010.

de Boer, B., Stocchi, P., Whitehouse, P. L., and van de Wal, R. S.: Current state and future perspectives on coupled ice-sheet–sea-level modelling, Quaternary Sci. Rev., 169, 13–28, 2017.

de Fleurian, B., Werder, M. A., Beyer, S., Brinkerhoff, D. J., Delaney, I., Dow, C. F., Downs, J., Gagliardini, O., Hoffman, M. J., Hooke, R. L., et al.: SHMIP The subglacial hydrology model intercomparison Project, J. Glaciol., 64, 897–916, 2018.

Dow, C. F., Werder, M. A., Nowicki, S., and Walker, R. T.: Modeling Antarctic subglacial lake filling and drainage cycles, The Cryosphere, 10, 1381–1393, https://doi.org/10.5194/tc-10-1381-2016, 2016.

Edwards, T. L., Nowicki, S., Marzeion, B., Hock, R., Goelzer, H., Seroussi, H., Jourdain, N. C., Slater, D. A., Turner, F. E., Smith, C. J., McKenna, C. M., Simon, E., Abe-Ouchi, A., Gregory, J. M., Larour, E., Lipscomb, W. H., Payne, A. J., Shepherd, A., Agosta, C., Alexander, P., Albrecht, T., Anderson, B., Asay-Davis, X., Aschwanden, A., Barthel, A., Bliss, A., Calov, R., Chambers, C., Champollion, N., Choi, Y., Cullather, R., Cuzzone, J., Dumas, C., Felikson, D., Fettweis, X., Fujita, K., Galton-Fenzi, B. K., Gladstone, R., Golledge, N. R., Greve, R., Hattermann, T., Hoffman, M. J., Humbert, A., Huss, M., Huybrechts, P., Immerzeel, W., Kleiner, T., Kraaijenbrink, P., Le clec'h, S., Lee, V., Leguy, G. R., Little, C. M., Lowry, D. P., Malles, J.-H., Martin, D. F., Maussion, F., Morlighem, M., O'Neill, J. F., Nias, I., Pattyn, F., Pelle, T., Price, S. F., Quiquet, A., Radić, V., Reese, R., Rounce, D. R., Rückamp, M., Sakai, A., Shafer, C., Schlegel, N.-J., Shannon, S., Smith, R. S., Straneo, F., Sun, S., Tarasov, L., Trusel, L. D., Van Breedam, J., van de Wal, R., van den Broeke, M., Winkelmann, R., Zekollari, H., Zhao, C., Zhang, T., and Zwinger, T.: Projected land ice contributions to twenty-first-century sea level rise, Nature, 593, 74–82, https://doi.org/10.1038/s41586-021-03302-y, 2021.

Fleurian, B. d., Gagliardini, O., Zwinger, T., Durand, G., Meur, E. L., Mair, D., and Råback, P.: A double continuum hydrological model for glacier applications, The Cryosphere, 8, 137–153, 2014.

Flowers, G. E.: Modelling water flow under glaciers and ice sheets, Proceedings of the Royal Society of London A: Mathematical, Phys. Eng. Sci., 471, 20140907, https://doi.org/10.1098/rspa.2014.0907, 2015.

Flowers, G. E. and Clarke, G. K. C.: A Multicomponent Coupled Model of Glacier Hydrology: 1. Theory and Synthetic Examples, J. Geophys. Res., 107, ECV-9, https://doi.org/10.1029/2001JB001122, 2002a.

Frederikse, T., Buchanan, M. K., Lambert, E., Kopp, R. E., Oppenheimer, M., Rasmussen, D., and van de Wal, R. S.: Antarctic Ice Sheet and emission scenario controls on 21st-century extreme sea-level changes, Nat. Commun., 11, 1–11, 2020.

Fretwell, P., Pritchard, H. D., Vaughan, D. G., Bamber, J. L., Barrand, N. E., Bell, R., Bianchi, C., Bingham, R. G., Blankenship, D. D., Casassa, G., Catania, G., Callens, D., Conway, H., Cook, A. J., Corr, H. F. J., Damaske, D., Damm, V., Ferraccioli, F., Forsberg, R., Fujita, S., Gim, Y., Gogineni, P., Griggs, J. A., Hindmarsh, R. C. A., Holmlund, P., Holt, J. W., Jacobel, R. W., Jenkins, A., Jokat, W., Jordan, T., King, E. C., Kohler, J., Krabill, W., Riger-Kusk, M., Langley, K. A., Leitchenkov, G., Leuschen, C., Luyendyk, B. P., Matsuoka, K., Mouginot, J., Nitsche, F. O., Nogi, Y., Nost, O. A., Popov, S. V., Rignot, E., Rippin, D. M., Rivera, A., Roberts, J., Ross, N., Siegert, M. J., Smith, A. M., Steinhage, D., Studinger, M., Sun, B., Tinto, B. K., Welch, B. C., Wilson, D., Young, D. A., Xiangbin, C., and Zirizzotti, A.: Bedmap2: improved ice bed, surface and thickness datasets for Antarctica, The Cryosphere, 7, 375–393, https://doi.org/10.5194/tc-7-375-2013, 2013.

Gagliardini, O. and Werder, M. A.: Influence of increasing surface melt over decadal timescales on land-terminating Greenland-type outlet glaciers, J. Glaciol., 64, 700–710, 2018.

Gandy, N., Gregoire, L. J., Ely, J. C., Cornford, S. L., Clark, C. D., and Hodgson, D. M.: Exploring the ingredients required to successfully model the placement, generation, and evolution of ice streams in the British-Irish Ice Sheet, Quaternary Sci. Rev., 223, 105915, https://doi.org/10.1016/j.quascirev.2019.105915, 2019.

Gillet-Chaulet, F., Durand, G., Gagliardini, O., Mosbeux, C., Mouginot, J., Rémy, F., and Ritz, C.: Assimilation of surface velocities acquired between 1996 and 2010 to constrain the form of the basal friction law under Pine Island Glacier, Geophys. Res. Lett., 43, 10–311, 2016.

Goeller, S., Thoma, M., Grosfeld, K., and Miller, H.: A balanced water layer concept for subglacial hydrology in large-scale ice sheet models, The Cryosphere, 7, 1095–1106, https://doi.org/10.5194/tc-7-1095-2013, 2013.

Golledge, N. R., Kowalewski, D. E., Naish, T. R., Levy, R. H., Fogwill, C. J., and Gasson, E. G. W.: The multi-millennial Antarctic commitment to future sea-level rise, Nature, 526, 421–425, 2015.

Hewitt, I. J.: Modelling distributed and channelized subglacial drainage: the spacing of channels, J. Glaciol., 57, 302–314, 2011.

Hewitt, I. J., Schoof, C., and Werder, M. A.: Flotation and free surface flow in a model for subglacial drainage. Part 2. Channel flow, J. Fluid Mech., 702, 157–187, 2012.

Hoffman, M. and Price, S.: Feedbacks between coupled subglacial hydrology and glacier dynamics, J. Geophys. Res.-Earth Surface, 119, 414–436, 2014.

ISMIP6 committee: Ice Sheet Model Intercomparison Project for CMIP6 (ISMIP6) wiki page, https://www.climate-cryosphere.org/wiki/index.php?title=ISMIP6_wiki_page (last access: 1 March 2022), 2022.

Joughin, I., Smith, B. E., and Schoof, C. G.: Regularized Coulomb Friction Laws for Ice Sheet Sliding: Application to Pine Island Glacier, Antarctica, Geophys. Res. Lett., 46, 4764–4771, https://doi.org/10.1029/2019GL082526, 2019.

Jourdain, N. C., Asay-Davis, X., Hattermann, T., Straneo, F., Seroussi, H., Little, C. M., and Nowicki, S.: A protocol for calculating basal melt rates in the ISMIP6 Antarctic ice sheet projections, The Cryosphere, 14, 3111–3134, https://doi.org/10.5194/tc-14-3111-2020, 2020.

Kazmierczak, E., Sun, S., Coulon, V., and Pattyn, F.: Subglacial hydrology modulates basal sliding response of the

Antarctic ice sheet to climate forcing, Zenodo [data set], https://doi.org/10.5281/zenodo.7118690, 2022.

Kopp, R., DeConto, R., Bader, D., Horton, R., Hay, C., Kulp, S., Oppenheimer, M., Pollard, D., and Strauss, B.: Implications of ice-shelf hydrofracturing and ice cliff collapse mechanisms for sea-level projections, arXiv [preprint], https://doi.org/10.48550/arXiv.1704.05597,, 2017.

Kopp, R. E., Horton, R. M., Little, C. M., Mitrovica, J. X., Oppenheimer, M., Rasmussen, D., Strauss, B. H., and Tebaldi, C.: Probabilistic 21st and 22nd century sea-level projections at a global network of tide-gauge sites, Earth's Future, 2, 383–406, 2014.

Le Brocq, A., Payne, A., Siegert, M., and Alley, R.: A subglacial water-flow model for West Antarctica, J. Glaciol., 55, 879–888, https://doi.org/10.3189/002214309790152564, 2009.

Le Brocq, A. M., Payne, A. J., and Siegert, M. J.: West Antarctic Balance Calculations: Impact of Flux-Routing Algorithm, Smoothing Algorithm and Topography, Comput. Geosci., 32, 1780–1795, 2006.

Lüthi, M., Funk, M., Iken, A., Gogineni, S., and Truffer, M.: Mechanisms of fast flow in Jakobshavn Isbræ, West Greenland: Part III. Measurements of ice deformation, temperature and cross-borehole conductivity in boreholes to the bedrock, J. Glaciol., 48, 369–385, https://doi.org/10.3189/172756502781831322, 2002.

Martin, M. A., Winkelmann, R., Haseloff, M., Albrecht, T., Bueler, E., Khroulev, C., and Levermann, A.: The Potsdam Parallel Ice Sheet Model (PISM-PIK) – Part 2: Dynamic equilibrium simulation of the Antarctic ice sheet, The Cryosphere, 5, 727–740, https://doi.org/10.5194/tc-5-727-2011, 2011.

Mengel, M. and Levermann, A.: Ice plug prevents irreversible discharge from East Antarctica, Nat. Clim. Change, 4, 451–455, https://doi.org/10.1038/nclimate2226, 2014.

Morlighem, M.: MEaSUREs BedMachine Antarctica, Version 2, Boulder, Colorado USA, NASA National Snow and Ice Data Center Distributed Active Archive Center [data set], https://doi.org/10.5067/E1QL9HFQ7A8M, 2020.

Morlighem, M., Rignot, E., Binder, T., Blankenship, D., Drews, R., Eagles, G., Eisen, O., Ferraccioli, F., Forsberg, R., Fretwell, P., Forsberg, R., Fretwell, P., Goel, V., Greenbaum,J. S., Gudmundsson, H., Guo, J., Helm, V., Hofstede, C., Howat, I., Humbert, A., Jokat, W., Karlsson, N. B., Lee, W. S., Matsuoka, K., Millan, R., Mouginot, J., Paden, J., Pattyn, F., Roberts, J., Rosier, S., Ruppel, A., Seroussi, H., Smith, E. C., Steinhage, D., Sun, B., van den Broeke, M. R., van Ommen, T. D., van Wessem, M., and Young, D. A.: Deep glacial troughs and stabilizing ridges unveiled beneath the margins of the Antarctic ice sheet, Nat. Geosci., 13, 132–137, 2020.

Muto, A., Alley, R. B., Parizek, B. R., and Anandakrishnan, S.: Bed-type variability and till (dis) continuity beneath Thwaites Glacier, West Antarctica, Ann. Glaciol., 60, 82–90, 2019.

Nowicki, S. M. J., Payne, A., Larour, E., Seroussi, H., Goelzer, H., Lipscomb, W., Gregory, J., Abe-Ouchi, A., and Shepherd, A.: Ice Sheet Model Intercomparison Project (ISMIP6) contribution to CMIP6, Geosci. Model Dev., 9, 4521–4545, https://doi.org/10.5194/gmd-9-4521-2016, 2016.

Pattyn, F.: Numerical Modelling of a Fast-Flowing Outlet Glacier: Experiments with Different Basal Conditions, Ann. Glaciol., 23, 237–246, 1996.

Pattyn, F.: Sea-level response to melting of Antarctic ice shelves on multi-centennial timescales with the fast Elementary Thermomechanical Ice Sheet model (f.ETISh v1.0), The Cryosphere, 11, 1851–1878, https://doi.org/10.5194/tc-11-1851-2017, 2017.

Pattyn, F. and Durand, G.: Why marine ice sheet model predictions may diverge in estimating future sea level rise, Geophys. Res. Lett., 40, 4316–4320, https://doi.org/10.1002/grl.50824, 2013.

Pattyn, F., De Brabander, S., and Huyghe, A.: Basal and Thermal Control Mechanisms of the Ragnhild Glaciers, East Antarctica, Ann. Glaciol., 40, 225–231, 2005.

Pattyn, F., Perichon, L., Durand, G., Favier, L., Gagliardini, O., Hindmarsh, R. C., Zwinger, T., Albrecht, T., Cornford, S., Docquier, D., Fürst, J. J., Goldberg, D., Gudmundsson, G. H., Humbert, A., Hütten, M., Huybrechts, P., Jouvet, G., Kleiner, T., Larour, E., Martin, D., Morlighem, M., Payne, A. J., Pollard, D., Rückamp, M., Rybak, O., Seroussi, H., Thoma, M., and Wilkens, N.: Grounding-line migration in plan-view marine ice-sheet models: results of the ice2sea MISMIP3d intercomparison, J. Glaciol., 59, 410–422, https://doi.org/10.3189/2013JoG12J129, 2013.

Pelletier, C., Klein, F., Zipf, L., Haubner, K., Mathiot, P., Pattyn, F., Moravveji, E., and Vanden Broucke, S.: PARASO source code (no COSMO) (v1.4.2), Zenodo [code], https://doi.org/10.5281/zenodo.5337510, 2021.

Pelletier, C., Fichefet, T., Goosse, H., Haubner, K., Helsen, S., Huot, P.-V., Kittel, C., Klein, F., Le clec'h, S., van Lipzig, N. P. M., Marchi, S., Massonnet, F., Mathiot, P., Moravveji, E., Moreno-Chamarro, E., Ortega, P., Pattyn, F., Souverijns, N., Van Achter, G., Vanden Broucke, S., Vanhulle, A., Verfaillie, D., and Zipf, L.: PARASO, a circum-Antarctic fully coupled ice-sheet–ocean–sea-ice–atmosphere–land model involving f.ETISh1.7, NEMO3.6, LIM3.6, COSMO5.0 and CLM4.5, Geosci. Model Dev., 15, 553–594, https://doi.org/10.5194/gmd-15-553-2022, 2022.

Pollard, D. and DeConto, R. M.: Description of a hybrid ice sheet-shelf model, and application to Antarctica, Geosci. Model Dev., 5, 1273–1295, https://doi.org/10.5194/gmd-5-1273-2012, 2012a.

Pollard, D. and DeConto, R. M.: A simple inverse method for the distribution of basal sliding coefficients under ice sheets, applied to Antarctica, The Cryosphere, 6, 953–971, https://doi.org/10.5194/tc-6-953-2012, 2012b.

Rignot, E., Mouginot, J., Scheuchl, B., van den Broeke, M., van Wessem, M. J., and Morlighem, M.: Four decades of Antarctic Ice Sheet mass balance from 1979–2017, P. Natl. Acad. Sci., 116, 1095–1103, https://doi.org/10.1073/pnas.1812883116, 2019.

Ritz, C., T. L. Edwards a, d. G. D., Payne, A. J., Peyaud, V., and Hindmarsh, R. C. A.: Potential sea-level rise from Antarctic ice-sheet instability constrained by observations, Nature, 528, 115–118, https://doi.org/10.1038/nature16147, 2015.

Robel, A. A., Wilson, E., and Seroussi, H.: Layered seawater intrusion and melt under grounded ice, The Cryosphere, 16, 451–469, https://doi.org/10.5194/tc-16-451-2022, 2022.

Scambos, T. A., Bell, R. E., Alley, R. B., Anandakrishnan, S., Bromwich, D., Brunt, K., Christianson, K., Creyts, T., Das, S., DeConto, R., Dutrieux, P., Fricker, H. A., Holland, D., MacGregor, J., Medley, B., Nicolas, J. P., Pollard, D., Siegfried, M. R., Smith, A. M., Steig, E. J., Trusel, L. D., Vaughan, D. G., and Yager, P. L.: How much, how fast?: A science review and outlook for research on the instability of Antarctica's Thwaites Glacier in the 21st century, Global Planet. Change, 153, 16–34, 2017.

Schoof, C.: Ice sheet grounding line dynamics: Steady states, stability, and hysteresis, J. Geophys. Res.-Earth Surface, 112, f03S28, https://doi.org/10.1029/2006JF000664, 2007.

Schoof, C.: Ice-sheet acceleration driven by melt supply variability, Nature, 468, 803–806, 2010.

Schoof, C., Hewitt, I. J., and Werder, M. A.: Flotation and free surface flow in a model for subglacial drainage. Part 1. Distributed drainage, J. Fluid Mech., 702, 126–156, 2012.

Seroussi, H., Nowicki, S., Payne, A. J., Goelzer, H., Lipscomb, W. H., Abe-Ouchi, A., Agosta, C., Albrecht, T., Asay-Davis, X., Barthel, A., Calov, R., Cullather, R., Dumas, C., Galton-Fenzi, B. K., Gladstone, R., Golledge, N. R., Gregory, J. M., Greve, R., Hattermann, T., Hoffman, M. J., Humbert, A., Huybrechts, P., Jourdain, N. C., Kleiner, T., Larour, E., Leguy, G. R., Lowry, D. P., Little, C. M., Morlighem, M., Pattyn, F., Pelle, T., Price, S. F., Quiquet, A., Reese, R., Schlegel, N.-J., Shepherd, A., Simon, E., Smith, R. S., Straneo, F., Sun, S., Trusel, L. D., Van Breedam, J., van de Wal, R. S. W., Winkelmann, R., Zhao, C., Zhang, T., and Zwinger, T.: ISMIP6 Antarctica: a multi-model ensemble of the Antarctic ice sheet evolution over the 21st century, The Cryosphere, 14, 3033–3070, https://doi.org/10.5194/tc-14-3033-2020, 2020.

Shapiro, N. M. and Ritzwoller, M. H.: Inferring Surface Heat Flux Distributions Guided by a Global Seismic Model: Particular Application to Antarctica, Earth Planet. Sci. Lett., 223, 213–224, 2004.

Shepherd, A., Gilbert, L., Muir, A. S., Konrad, H., McMillan, M., Slater, T., Briggs, K. H., Sundal, A. V., Hogg, A. E., and Engdahl, M. E.: Trends in Antarctic Ice Sheet elevation and mass, Geophys. Res. Lett., 46, 8174–8183, 2019.

Sommers, A., Rajaram, H., and Morlighem, M.: SHAKTI: Subglacial Hydrology and Kinetic, Transient Interactions v1.0, Geosci. Model Dev., 11, 2955–2974, https://doi.org/10.5194/gmd-11-2955-2018, 2018.

Sun, S., Pattyn, F., Simon, E. G., Albrecht, T., Cornford, S., Calov, R., Dumas, C., Gillet-Chaulet, F., Goelzer, H., Golledge, N. R., Greve, R., Hoffman, M. J., Humbert, A., Kazmierczak, E., Kleiner, T., Leguy, G. R., Lipscomb, W. H., Martin, D., Morlighem, M., Nowicki, S., Pollard, D., Price, S., Quiquet, A., Seroussi, H., Schlemm, T., Sutter, J., van de Wal, R. S. W., Winkelmann, R., and Zhang, T.: Antarctic ice sheet response to sudden and sustained ice-shelf collapse (ABUMIP), J. Glaciol., 66, 891–904, https://doi.org/10.1017/jog.2020.67, 2020.

Tsai, V. C., Stewart, A. L., and Thompson, A. F.: Marine ice-sheet profiles and stability under Coulomb basal conditions, J. Glaciol., 61, 205–215, https://doi.org/10.3189/2015JoG14J221, 2015.

Tulaczyk, S. M., Kamb, B., and Engelhardt, H. F.: Basal Mechanics of Ice Stream B, West Antarctica. I. Till Mechanics, J. Geophys. Res., 105, 463–481, 2000.

Van der Veen, C. J.: Longitudinal Stresses and Basal Sliding: a Comparative Study, in: Dynamics of the West Antarctic Ice Sheet, edited by: Van der Veen, C. and Oerlemans, J., pp. 223–248, Dordrecht, Kluwer Academic Publishers, 1987.

van der Wel, N., Christoffersen, P., and Bougamont, M.: The influence of subglacial hydrology on the flow of Kamb Ice Stream, West Antarctica, J. Geophys. Res.-Earth Surface, 118, 97–110, https://doi.org/10.1029/2012JF002570, 2013.

van Pelt, W. J. and Oerlemans, J.: Numerical simulations of cyclic behaviour in the Parallel Ice Sheet Model (PISM), J. Glaciol., 58, 347–360, https://doi.org/10.3189/2012JoG11J217, 2012.

Van Wessem, J., Reijmer, C., Morlighem, M., Mouginot, J., Rignot, E., Medley, B., Joughin, I., Wouters, B., Depoorter, M., Bamber, J., Lenaerts, J., De Van Berg, W., Van Den Broeke, M., and Van Meijgaard, E.: Improved representation of East Antarctic surface mass balance in a regional atmospheric climate model, J. Glaciol., 60, 761–770, https://doi.org/10.3189/2014JoG14J051, 2014.

Walder, J. S.: Stability of Sheet Flow of Water Beneath Temperate Glaciers and Implications for Glacier Surging, J. Glaciol., 28, 273–293, 1982.

Weertman, J.: On the Sliding of Glaciers, J. Glaciol., 3, 33–38, 1957.

Weertman, J.: Effect of a Basal Water Layer on the Dimensions of Ice Sheets, J. Glaciol., 6, 191–207, https://doi.org/10.3189/S0022143000019213, 1966.

Weertman, J.: General Theory of Water Flow at the Base of a Glacier or Ice Sheet, Rev. Geophys., 10, 287–333, 1972.

Weertman, J. and Birchfield, G. E.: Subglacial Water Flow under Ice Streams and West Antarctic Ice Sheet Stability, Ann. Glaciol., 3, 316–320, 1982.

Werder, M. A., Hewitt, I. J., Schoof, C. G., and Flowers, G. E.: Modeling channelized and distributed subglacial drainage in two dimensions, J. Geophys. Res.-Earth Surface, 118, 2140–2158, 2013.

Winkelmann, R., Martin, M. A., Haseloff, M., Albrecht, T., Bueler, E., Khroulev, C., and Levermann, A.: The Potsdam Parallel Ice Sheet Model (PISM-PIK) – Part 1: Model description, The Cryosphere, 5, 715–726, https://doi.org/10.5194/tc-5-715-2011, 2011.